TB, BPN, MST/204196, 12/12/2005

INSTITUTE OF PHYSICS PUBLISHING MEASUREMENT SCIENCE AND TECHNOLOGY

Meas. Sci. Technol. **16** (2005) 1–8 doi:10.1088/0957-0233/16/0/000

The development of optical techniques for the measurement of pressure and skin friction

Sergey Fonov, Grant Jones, Jim Crafton, Vladimir Fonov and Larry Goss

Innovative Scientific Solutions, Inc., 2766 Indian Ripple Rd, Dayton OH 45440, USA

E-mail: gosslp@innssi.com

Received 12 July 2005, in final form 9 November 2005
Published DD MMM 2005
Online at stacks.iop.org/MST/16/1

Abstract

A novel measurement approach is described which has been developed to allow both pressure and skin friction measurements at very low speeds in liquid or gaseous environments. This approach, surface stress-sensitive films, S^3F, is based on the deformation of an elastic media and the transformation of this deformation into surface loads (pressure and shear stresses). Measurements in both air and water flows have been made. A comparative analysis of the S^3F and PSP techniques for a low-speed air-flow case is presented.

Keywords: pressure, skin friction, flow visualization, contact loads, laser induced flourescence, cross-correlation, 3D deformations, flow diagnostics, contact pressure sensing, water and wind tunnel diagnostics

(Some figures in this article are in colour only in the electronic version)

1. Introduction

Traditional techniques for making measurements of surface temperature and pressure on wind-tunnel models utilize embedded arrays of thermocouples and pressure taps. This approach requires significant model construction and set-up time while producing data with limited spatial resolution. Furthermore, physical constraints such as mechanical movement or section thickness can preclude the use of thermocouples and pressure taps in certain regions of a model. An alternative approach that has received considerable attention during the past 15 years is the use of luminescent probes that are sensitive to temperature and pressure. These techniques, known as temperature (TSP) and pressure-sensitive paint (PSP), have resulted in high-spatial-resolution measurements of temperature and pressure on surfaces that were formerly inaccessible [1].

While PSP has demonstrated significant potential in high-speed wind tunnels, several issues that limit the accuracy of the technique have been identified [1–3]. Among these issues are errors due to model displacement and deformation, instability of the illumination source, photo-degradation and sedimentation of the painted surface and non-uniform temperatures on the model surface. Binary-paint systems were developed to address the errors associated with standard PSP. These systems consist of two probes—a pressure probe and a reference probe. The pressure probe is sensitive to illumination, pressure and temperature, while the reference probe is sensitive to illumination and temperature. By taking the appropriate ratios, temperature-independent pressure measurements can be made successfully. While binary systems have extended the useful velocity range for PSP into the 10–20 m s^{-1} range, lower velocities require a more sensitive technique.

A new technique based on the deformation of an elastic media and the transformation of this deformation into surface loads (pressure and shear stresses) called surface stress-sensitive film (S^3F) has been developed by the authors. Measurements in both air and water flows have been made. Because the technique does not depend on oxygen quenching, many of the limitations of PSP have been overcome.

The hardware platform for S^3F is very similar to PSP and includes a surface- or volume-distributed transducer, a specialized light source, an image-acquisition system, and dedicated data-acquisition and -analysis software. Data-processing algorithms for these imaging based techniques

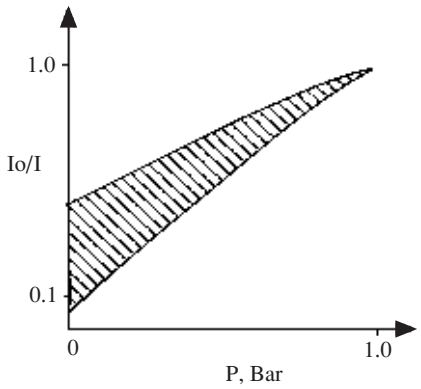

Figure 1. Stern–Vormer plot of various PSPs.

have many common steps: i.e., image alignment using cross-correlation techniques, image resection and image filtering. A detailed discussion of the S^{3}F technique is as follows.

2. S^{3}F measurement technique

It should be emphasized that PSPs based on oxygen quenching are essentially absolute pressure gauges. The sensitivity of a PSP $[\mathrm{d}(I\mathrm{o}/I)/\mathrm{d}P]$ is a function of the total pressure, which decreases as $1/P^2$, implying that low-speed (high-pressure) measurements will be difficult.

The sensitivity of most currently available PSP formulations varies from 50 to 100% of the intensity per bar (see figure 1) and cannot be increased significantly by modification of the physical and/or photochemical properties of the PSP. This creates a significant problem for low-speed PSP applications where pressure variations are relatively small [4, 5]. A typical example is the pressure field generated at very low velocities—Mach numbers below 0.05. Since pressure variations on the model are proportional to the square of the Mach number, the range of pressure variation δP at Ma $= 0.05$ ($V = 35$ mph) is relatively small (100 Pa). This value is approximately one hundred times less than that observed at the high-speed flow condition of $M = 0.5$ ($V = 350$ mph and $\delta P = 10^4$ Pa). Since the sensitivity of the PSP cannot be modified for the low-speed case, one can obtain reliable results only by increasing the signal-to-noise ratio of the acquired data (averaging many images) and compensating for all error sources, i.e., illumination non-stability, model displacement and deformation and temperature effects. The temperature sensitivity of single component PSPs varies between 100 Pa $^\circ$C^{-1} and 1000 Pa $^\circ$C^{-1} which is comparable to the total pressure range for the Ma $= 0.05$ case. Binary paint systems allow temperature-independent pressure measurements; however, the pressure sensitivity of these systems is no better than that of standard PSPs. Because of these constraints, PSP measurements at flow velocities below Ma $= 0.05$ have been semi-quantitative, and significant experimental efforts have been required to reduce measurement errors. A more sensitive pressure-sensing technique, surface shear-sensitive film (S^{3}F), has been developed for speeds below Mach 0.05.

A standard approach for achieving high measurement accuracy is to increase the sensitivity of a gauge by measuring increments relative to a fixed value, e.g., using a differential pressure gauge instead of an absolute pressure gauge. The idea of making differential pressure measurements is the cornerstone of the S^{3}F measurement technique. The origin of the S^{3}F technique began in the early 1990s as a direct method to measure surface shear force [6, 7]. This approach consisted of mounting on the model surface a sensing element in the form of a thin film made of a flexible elastomer of known thickness and shear modulus. Markers were applied to the film and the model surface, and an interference method was used to measure the shear deformation of the film caused by flow. The shearing stress was determined using Hooke's law for shear strain. The main drawback of this original approach was related to the fact that gradients of the normal pressure can also create shear displacement of the elastomer, and thus they need to be taken into account [8]. These small gradients in the normal component of force, however, are the quantities that we are trying to detect at low speeds. To account for all the loads applied to an elastomer (pressure and shear) requires a measure of the full three-dimensional (3D) deformation of the film.

An elastomer behaves in the same manner as a non-compressible fluid; however, unlike standard fluids, it tries to recover its original shape after removal of the deformation force (see figure 2). Pressure loads P_1 and P_2 applied to adjacent surfaces will act to displace the elastic material, resulting in a change in the local thickness of value $\delta\Lambda \sim n_p(P_2 - P_1)$. This is a crude representation of the behaviour of the elastomer layer because, in general, the deformations of the layer are governed also by pressure gradients and shear forces.

The range of the linear frequency response of such an elastomer is limited by the natural frequency of the shear

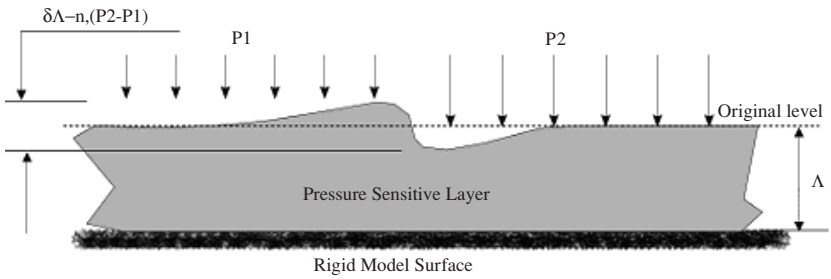

Figure 2. Realization of the differential principle.

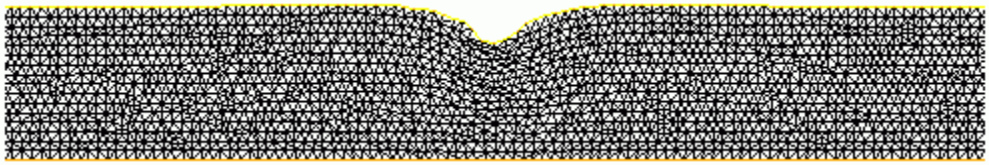

Figure 3. FEA solution of load on elastic polymer. Zoomed view of the deformed FEA grid.

oscillation and can be estimated as

$$f_0 \approx \frac{1}{2\pi}\sqrt{\frac{\mu}{\rho\Lambda^2}} \tag{1}$$

where μ is the shear stress module of the film, ρ the film density, and Λ the film thickness. By changing $\mu \in$ (100–1000) Pa and $\Lambda \in$ (0.1–1) mm, it is possible to adjust the frequency response of the film in the range 0.3–10 kHz which is ∼100 times better than that of standard PSP based on oxygen quenching.

For an S^{3}F layer to produce the desired results, it must be applied to the surface under study using techniques such as spraying the film with an airbrush, allowing the film to set up in a surface cavity on the model, and/or forming the film onto a Mylar film which can be placed onto a model surface. Forming films in model cavities or on Mylar allows control of the thickness and physical properties of the film. Forming the film consists of pouring its components into a flat cavity having a smooth or polished bottom. Following polymerization, the film is peeled off and placed on an airfoil to be studied. The film thickness can be estimated by direct measurements using either optical absorption or a capacitive thickness gauge. The film calibration procedure involves applying a specified load to the film surface and evaluating the film response function by measuring the corresponding normal and tangential deformation. The smaller the area to which the load is applied, the closer the response function of the film corresponds to an impulse function.

For simplicity, consider a one-dimensional load applied to the film surface. In this case the film deformations can be treated in two-dimensional (2D) space. A rectangular cavity on a plate with cross section [0, 20] × [0, 1] is filled with an S^{3}F film of thickness 1 mm. Constant loads (normal or tangential) are applied on the film interval [9.9, 10.1]. It is assumed that zero deformation occurs at the cavity walls (boundary condition).

Since S^{3}F is an elastic solid, it is deformed under an applied force. A point in the solid, originally at (x, y), is moved to (X, Y) upon application of a load. If the displacement vector $\vec{r} = (r_1, r_2) = (X - x, Y - y)$ is small, Hooke's law relates the stress tensor σ inside the solid to the deformation tensor ε [9]:

$$\sigma_{ij} = \lambda\delta_{ij}\nabla.\vec{r} + \mu\varepsilon_{ij}, \qquad \varepsilon_{ij} = \frac{1}{2}\left(\frac{\partial r_i}{\partial x_j} + \frac{\partial r_j}{\partial x_i}\right) \tag{2}$$

where δ_{ij} is the Kronecker symbol ($\delta_{ij} = 1$, if $i = j$, $\delta_{ij} = 0$, if $i \neq j$), and λ, μ are the two constants describing the material mechanical properties in terms of the modulus of elasticity E and Poisson ratio ν as

$$\lambda = \frac{E\nu}{(1+\nu)(1-2\nu)}, \qquad \mu = \frac{E}{(1+2\nu)}.$$

Writing the equation of elasticity in a form for the displacement vector $\vec{r}(x) \in \Omega$ yields

$$\int_\Omega [\mu\varepsilon_{ij}(\vec{r})\varepsilon_{ij}(\vec{w}) + \lambda\varepsilon_{ii}(\vec{r})\varepsilon_{jj}(\vec{w})] = \int_\Gamma \vec{\tau}\cdot\vec{w}, \qquad \forall\vec{w} \in \Omega \tag{3}$$

where the integrals are in volume Ω and on the volume boundary Γ [10].

A finite-element-analysis (FEA) solution of equation (3) for the case described above is presented in figure 3. A zoomed view of the deformed grid shows that the deformations are concentrated over the film surface in a region with a diameter that is approximately two to three times the thickness of the film layer.

Figure 4 presents plots of the normal and tangential deformations of an S^{3}F film that result from the action of a normal (figure 4(*a*)) and shear (figure 4(*b*)) applied load. Note that the application of either a normal or shear load to the elastomer surface results in both a normal and a tangential deformation of the film. The magnitude of the normal deformation is largest in the case of the applied normal load while the magnitude of the tangential deformtion is largest in the case of the applied tangential load; however, a certain amount of cross-talk occurs between components for elastomer films. This cross-talk is on the order of 10–20% of the main component and requires the measurement of both deformation components to determine the original applied load.

The normal deformation response $n_n(x)$ can be treated as a response to a normal load $\delta(x)$ applied to the surface. Similary, $n_s(x)$ is the tangential deformation response due to a normal load $\delta(x)$ applied to the surface. Applying the load $\delta(x)$ in the tangential direction creates the response functions $s_n(x)$ and $s_s(x)$ which describe the normal and tangential deformations, respectively. The elastic reaction, $\mathbf{R}(x) \equiv (R_x, R_y)$, can be expressed as the convolution of the response matrix $\mathbf{G}(x) = \begin{pmatrix} n_n & n_s \\ s_n & s_s \end{pmatrix}$ and the applied surface load, $\mathbf{L}(x) = (L_x, L_y)$, assuming a linear system [9, 10]:

$$\mathbf{R}(x) = \int \mathbf{G}(x - x')\mathbf{L}(x')\,\mathrm{d}x'. \tag{4}$$

If the response matrix $\mathbf{G}(x)$ can be determined experimentally or by FEA modelling, the applied loads, $\mathbf{L}(x)$, can be found by the deconvolution of equation (4):

$$\mathbf{L} = \mathbf{G}^{-1}\cdot\mathbf{R}. \tag{5}$$

To ascertain how the deconvolution is accomplished and the applied loads determined, the case of a simple normal and shear load applied to the surface will be examined. The normal displacement due to the action of a normal force can be approximated by the function

$$n_n(x) = \frac{1}{\mu}[(a_0 + a_1\exp(-|x|/k_1) + a_2\exp(-|x|/k_2)] \tag{6}$$

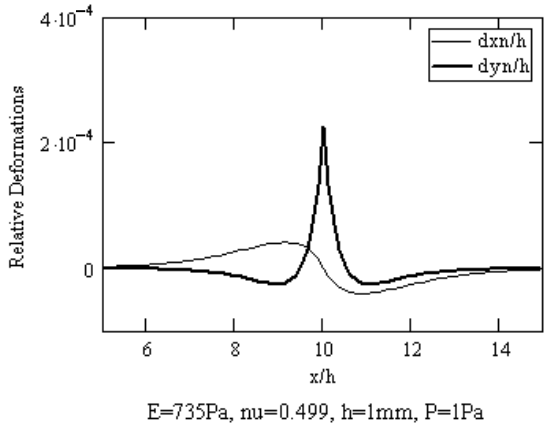

(*a*)

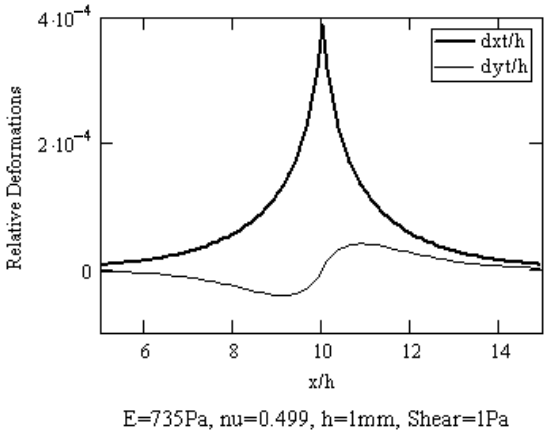

(*b*)

Figure 4. (*a*) Relative deformations due to application of 1 Pa normal load to elastomer surface. Layer thickness was $h = 1$ mm, elastic modulus was $E = 735$ Pa, Poisson ratio was $\nu = 0.499$, and load was applied at $x = 10$. Bold line represents normal deformation due to normal load. Thin line represents shear (tangential) deformation due to normal load. (*b*) Relative deformations due to application of 1 Pa shear load to elastomer surface. Layer thickness was $h = 1$ mm, elastic modulus was $E = 735$ Pa, Poisson ratio was $\nu = 0.499$, and load was applied at $x = 10$. Bold line represents shear (tangential) deformation due to shear load. Thin line represents normal deformation due to shear load.

where the parameters k_1, k_2 and a_i are obtained by fitting the experimental data or by FEA modelling. The shear (tangential) deformation due to the action of an applied normal force can be approximated by the function

$$n_s(x) = \frac{1}{\mu}(a_3 + a_4 x \exp(-|x|/k_3). \tag{7}$$

Similarly for the case of an applied shear load, the approximations for normal s_n and shear (tangential) s_s deformations are given by

$$s_n(x) = \frac{1}{\mu}(a_5 + a_6 x \exp(-|x|/k_4) \tag{8}$$

$$s_s(x) = \frac{1}{\mu}[(a_7 + a_8 \exp(-|x|/k_5 + a_9 \exp(-|x|/k_6)))]. \tag{9}$$

Rewriting equation (4) in a discrete form for the reaction to an arbitrary load $Lj = (Lnj, Lsj)$ applied at surface location

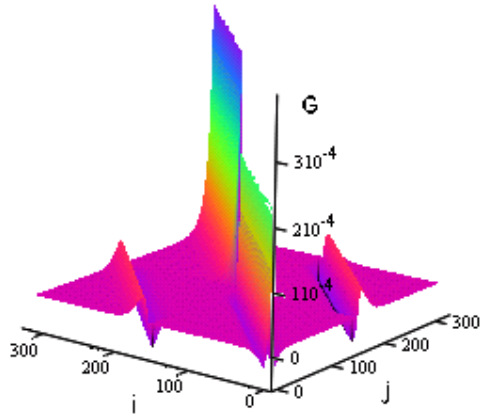

Figure 5. 3D presentation of G matrix.

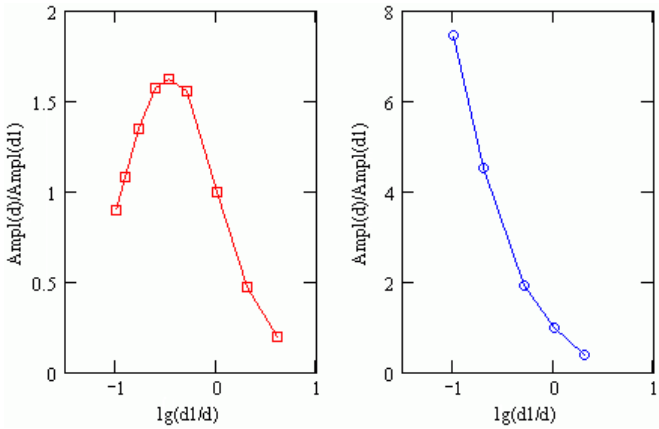

Figure 6. Estimation of AFC for normal (left) and tangential (right) loads.

$[x_0, x_N]$ yields

$$R_{nj} = \Delta x \sum_{k=0}^{N} L_{nk}\tilde{n}_n(x_j - x_k) + L_{sk}\tilde{s}_n(x_j - x_k) \tag{10}$$

$$R_{sj} = \Delta x \sum_{k=0}^{N} L_{nk}\tilde{n}_s(x_j - x_k) + L_{sk}\tilde{s}_s(x_j - x_k). \tag{11}$$

This system of linear equations (10–11) with unknown L_k has the diagonally dominant matrix (figure 5)

$$\mathbf{G}_{jk} = \begin{pmatrix} n_{njk} & s_{njk} \\ n_{sjk} & s_{sjk} \end{pmatrix} \tag{12}$$

which can be inverted and used to solve for the original loads (see equation (5)).

The response functions (equations (10)–(11)) depend on the thickness of the elastic film. The plots shown in figure 6 contain results obtained from FEA modelling of the response to harmonic normal and tangential (shear) loads applied at the interval d on an S^{3}F with a thickness d_1. The maximum deformations as a function of d_1/d can be treated as a measure of the spatial amplitude–frequency characteristics (AFC) of an S^{3}F film. The AFC for the normal (red line) and tangential (blue line) loads are quite different, especially at low d_1/d; thus, by varying the thickness of the layer, the sensitivity to either normal (pressure) or shear forces can be adjusted. Thick films favour the measurement of shear, while thin films favour the measurement of pressure.

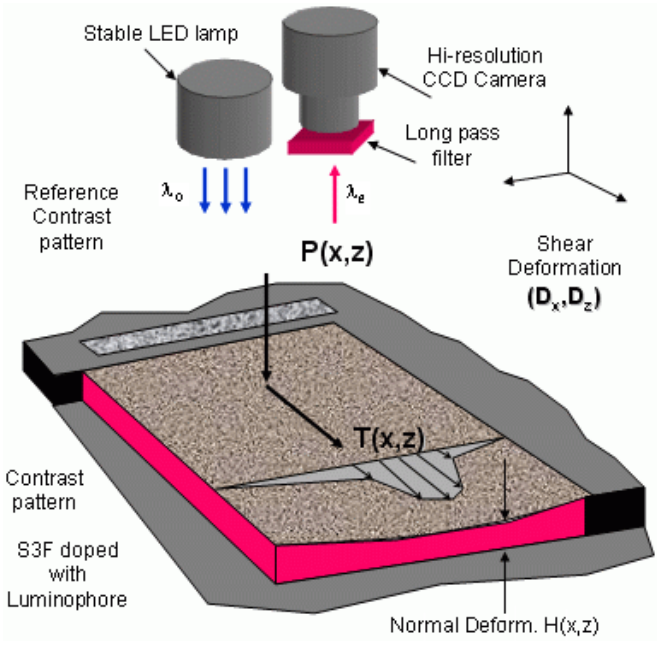

Figure 7. General layout of S^{3}F image acquisition system.

The experimental set-up for S^{3}F measurements is shown in figure 7. All three deformation components can be extracted from a set of wind-off and wind-on images acquired by a single high-resolution CCD camera. The normal component in this configuration is measured using the luminescence signal from the S^{3}F. This requires a stable light source and at least a 12 bit CCD camera. Static measurements have been conducted using a QIMAGING RETIGA EX CCD camera having 1280 × 1024 pixels and 12 bit amplitude resolution and a PCO CCD camera having 1600 × 1200 pixels and 14 bit amplitude resolution in combination with an LED lamp (from ISSI, output at 406 nm or 460 nm).

The OMS 3.1 software package (from ISSI) is used for image processing and includes alignment of the wind-off and wind-on images, normalizing and calculation of the shear displacement fields. This software provides the model-displacement compensation as a rigid body, using additional information from markers located on the S^{3}F substrate.

The sensitivity of the S^{3}F should be adjusted in accordance with the range of the expected experimental surface forces. The maximum acceptable deformation of the surface under study should be kept low to minimize its influence on the flowfield. The relative normal deformations should be kept below 1–2% of the relative film thickness, and the film thickness should be kept to less than 1–10% of the characteristic thickness of the model.

3. S^{3}F characteristics

The shear stress module and film thickness are the main parameters that determine the sensitivity and spatial resolution of the S^{3}F technique. The shear module, μ, can be measured directly by applying a shear force to the film (with known thickness) and measuring the corresponding displacement. The response functions can be estimated using an FEA model, as described in the previous section. Practically, it is possible to create a stable S^{3}F having a shear-stress module in the range $\mu = 30$–3000 Pa. Figure 8 shows a calibration curve for a practical S^{3}F composition. This composition displays good linearity and a small hysteresis, which is on the order of the tangential-displacement measurement accuracy of $\sigma = 0.1$–0.3 μm. The total linear dynamic range of the displacement is $\sim$1000 μm, which is large compared with the S^{3}F layer thickness of 1730 μm.

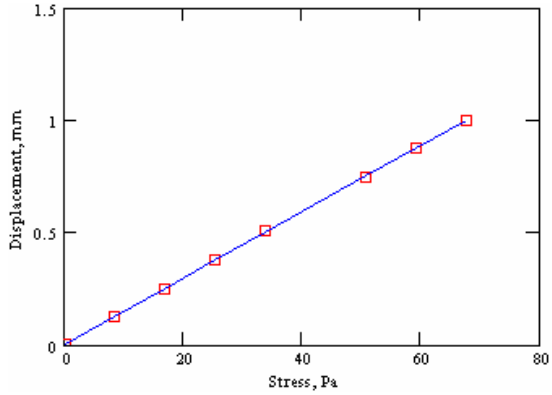

Figure 8. Calibration curve for S^{3}F composition with shear stress module $\mu = 117$ Pa.

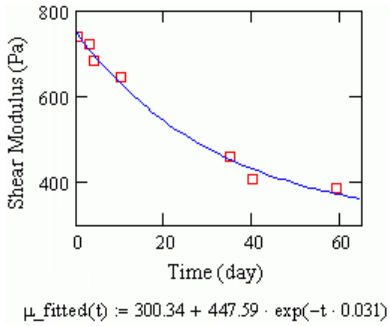

Figure 9. Decrease in shear modulus of S^{3}F film as a function of time. Film was 1 mm thick with an initial modulus of 735 Pa.

The actual film formulation is proprietary, however, it is based upon siloxane chemistry. The long term stability of the 1 mm S^{3}F films used in this study is shown in figure 9 as a function of time. The rate of modulus decay is $\sim$ 2% per day in the first 20 days, 1% per day in the 20–40 day period, and finally near 0% beyond 60 days. The total decrease in modulus over a 60 day period is approximately half of the original value. To ensure that this decrease has the minimal impact upon the measurement uncertainty, the modulus is measured before and after the experiment. If this is not possible, it is best to allow the film to approach its long-term value before use.

4. S^{3}F evaluation tests

All evaluation tests discussed in this paper were conducted in wind tunnels. However, since the S^{3}F technique is not dependent upon oxygen quenching, it can also be used in water tunnels. Fonov *et al* [10] successfully demonstrated this capability on an S^{3}F coated delta wing in a water tunnel.

Simple models with known pressure and friction-force distributions were used for feasibility tests in this study. One such model is shown in figure 10. This model consists of a plate having a wedged leading edge, which was installed vertically in the test section floor at zero side angle. The

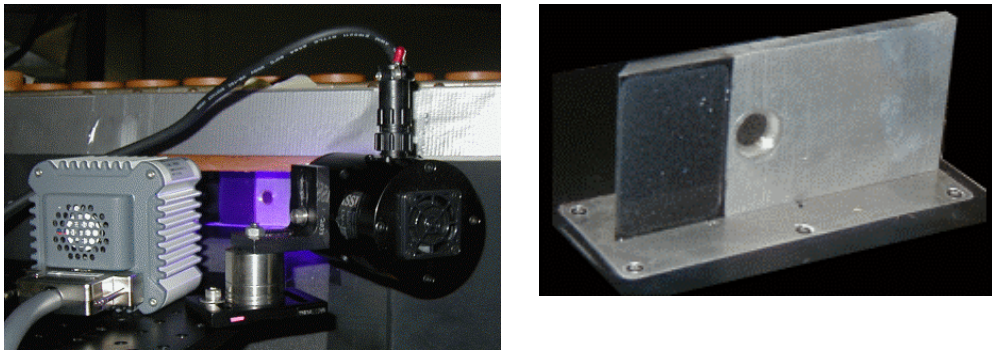

Figure 10. Typical S^3F experimental set-up (left). Tested model (right). S^3F cavity has depth of 1 mm (front black part).

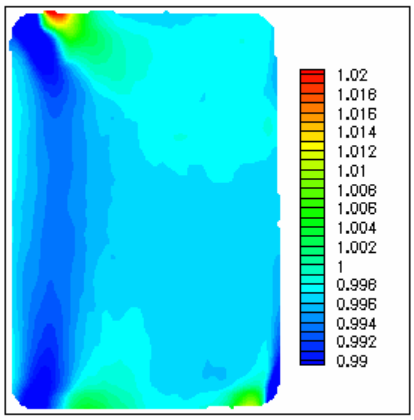

Figure 11. Normal deformation field (Io/I).

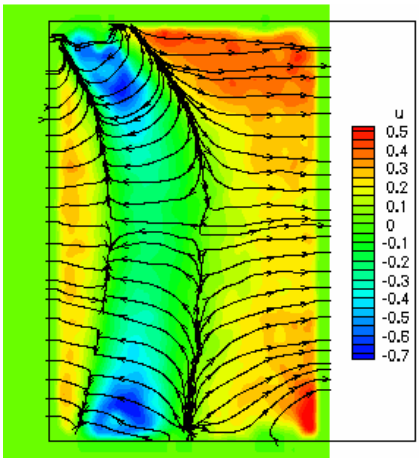

Figure 12. X-component of shear deformation field. Units are in pixels.

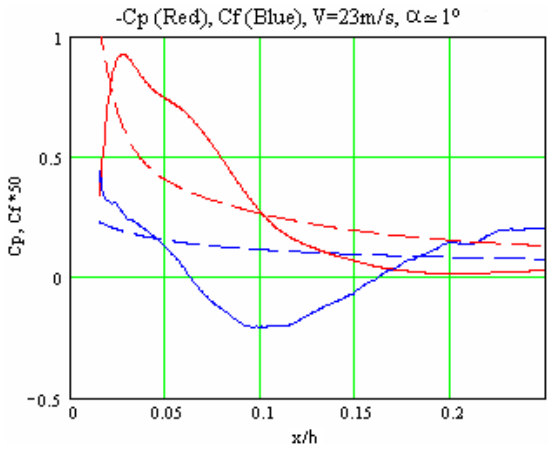

Figure 13. Reconstructed -Cp (red) and Cf*50 (blue) distributions compared with CFD (2D potential flow) and Blasius estimations (dashed Lines). $V = 23$ m s^{-1}, angle of attack $\alpha \cong 1^\circ$.

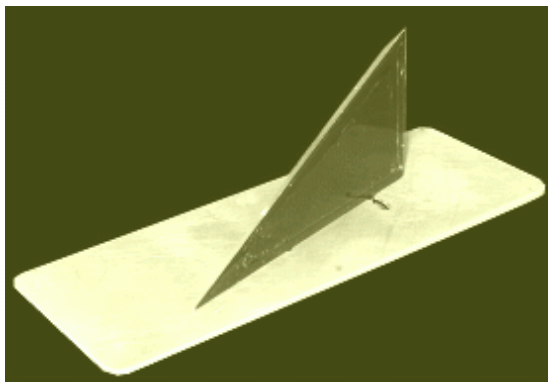

Figure 14. Delta-wing model.

plate has a cavity near the leading edge which was filled with S^3F. The experimental air-flow velocity varied from 10 to 20 m s^{-1}. The normal and shear deformation fields obtained at 20 m s^{-1} are presented in figures 11 and 12, respectively. The deformation field along the centre line can be considered to be two-dimensional, which allows the data-recovery scheme described previously to be used in this case. Figure 13 shows a comparison of the measured pressure and friction-force coefficients with estimates made by computational fluid dynamics (CFD). The magnitudes of the reconstructed loads are in good agreement with CFD results and Blasius estimations. The visible presence of a laminar bubble in the S^3F data explains the difference in the local load distributions. S^3F data near the leading edge are attenuated by the S^3F cavity boundaries.

A delta-wing model (figure 14) was also tested in the flow-velocity range 5–40 m s^{-1} and an angle of attack of 10°–15°. The upper surface cavity was filled with an S^3F with a thickness of 1 mm. Fine $Ti0_2$ powder was applied to the upper S^3F surface to create a pattern for shear-deformation measurements. A similar model coated with PSP was also tested to allow a comparison between S^3F and PSP data (figure 15).

The normal deformation distribution of the film is presented in figure 16. The vortex above the wing surface creates a narrow decompression region with a pressure gradient that is oriented across the ambient flow direction. This allows

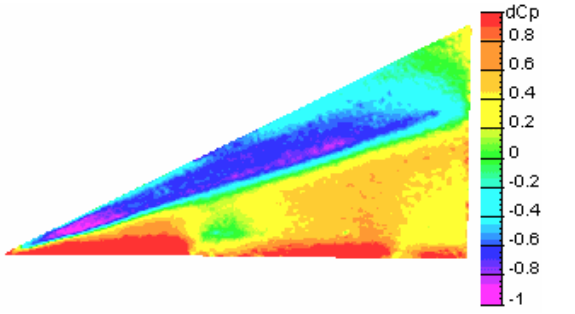

Figure 15. PSP results plotted in ΔC_p, $V = 20$ m s^{-1}, $\alpha = 10°$.

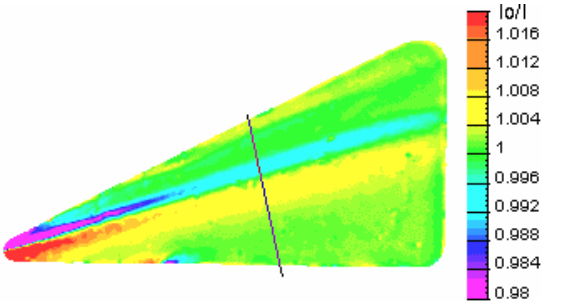

Figure 16. S^{3}F results: normal component of deformation field (Io/I); flow velocity 20 m s^{-1}, angle of attack $\alpha = 10°$.

each cross section of elastic deformation to be treated as a plane (two-dimensional). Figure 17 displays a comparison of PSP and S^{3}F data taken under nearly identical flow conditions. The sensitivity of the S^{3}F to pressure is about 25 times that of the PSP. Also only three images (one wind-off, one wind-on and one background) were required to obtain a good signal-to-noise ratio (SNR) for the S^{3}F case, as compared to 180 images for the PSP case.

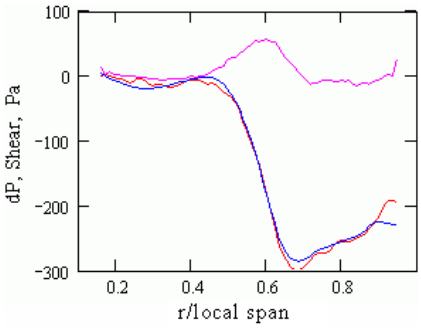

Figure 17. Comparison of S^{3}F (blue) data with PSP (red). Pressure variation in section presented in figure 16. Shear force represented by magenta curve.

Figure 18 illustrates pressure and shear-force-field measurements made on a coated plate under the action of a low-speed jet. S^{3}F with a thickness of 1 mm and shear modulus of $\mu = 270$ Pa was applied to the surface. A nozzle with internal diameter of 2 mm and axis inclined at the angle 40° created a low-speed jet flow. The normal component of the deformation field was measured using information from the luminescence output of the S^{3}F while the shear components were obtained using a cross-correlation technique. The combination of camera resolution (1280 × 1024 pixels) and subpixel-displacement routines provided shear displacement measurements with a resolution of 0.1 μm (cell window 32 × 32 pixel) with a dynamic range of ± 10 μm. A comparison of the S^{3}F data with pressure-tap results shows that the pressure field can be measured with a resolution of 3–5 Pa (defined by the SNR) for this S^{3}F composition.

The excellent agreement between the pressure taps results and the S^{3}F derived pressure data gives support to the one-dimensional pressure recovery approached used in this study. More complex model geometries would require more

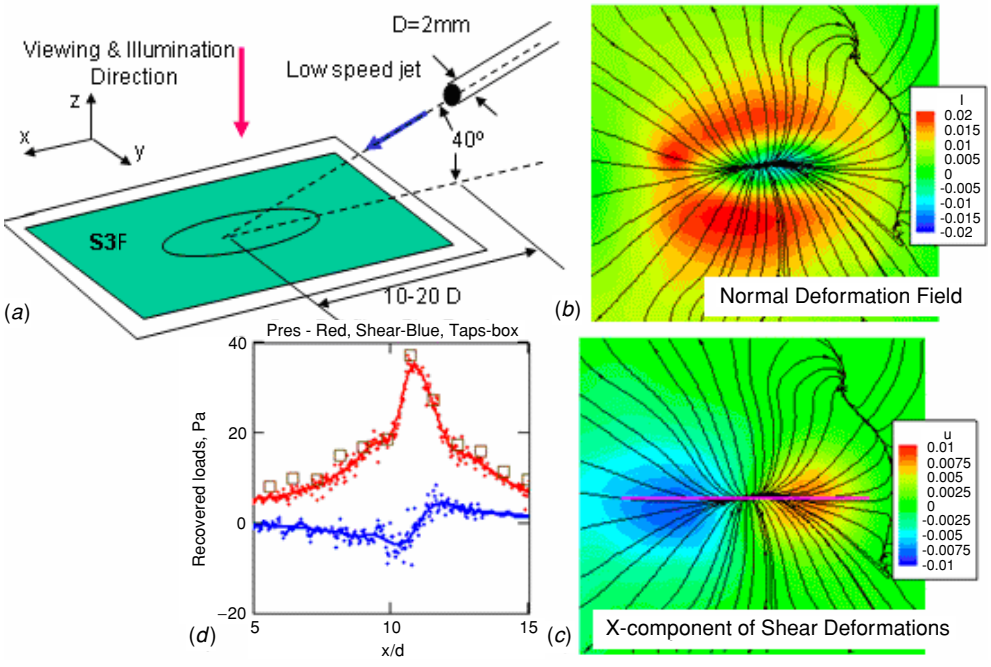

Figure 18. Impinging jet measurements of pressure and shear-force distributions using S^{3}F. (*a*) experimental set-up, (*b*) normal deformation field, (*c*) *x*-component of shear deformation and (*d*) S^{3}F derived shear (blue), pressure (red) and pressure taps (squares).

elaborate 2D and 3D recovery schemes. These more advanced approaches will be pursued in the near future.

5. Conclusions

A new sensor for the measurement of surface pressure and shear has been developed; this sensor is based on the 3D deformation of an elastic, incompressible film. The beneficial features of S^3F include the following: it does not depend on oxygen quenching and thus can work in most fluids; it acts as a differential pressure gauge; its sensitivity can be tuned to match the flow conditions; and it is sensitive to both shear and pressure components. Measurements of pressure and shear in several low-speed environments have been demonstrated using S^3F and the data compare favourably with results from binary PSP, CFD and pressure taps.

References

[1] Liu T, Campbell B, Burns S and Sullivan J 1997 Temperature and pressure-sensitive paints in aerodynamics *Appl. Mech. Rev.* **50** 227–46

[2] Liu T, Guille M and Sullivan J P 2001 Accuracy of pressure sensitive paint *AIAA J.* **39** 103–12

[3] Bell J H and McLachlan B G 1996 Image registration for pressure-sensitive paint applications *Exp. Fluids* **22** 78–86

[4] Mosharov V, Radchenko V and Fonov S 1997 *Luminescent Pressure Sensors in Aerodynamic Experiment* (Moscow: TsAGI, CWA Int Corp)

[5] Reda D V 1998 Measurements of continuous pressure and shear distributions using coating and imaging techniques *AIAA J.* **36** 895–9

[6] Tarasov V N and Orlov A A 1990 *Method for determining shear stress on aerodynamic model surface Patent of Russia* 4841553/23/1990

[7] Tarasov V, Fonov S and Morozov A 1997 New Gauges for Direct Skin Friction Measurements *Proc 17th Int. Congress on Instrumentation in Aerospace Simulation Facilities (ICIASF) (Monterey, CA, 29 Sept–2 Oct)*

[8] Landau L D and Lifshits E M 1995 *Course of Theoretical Physics: Theory of Elasticity* vol 7 (Boston, MA: Butterworth-Heinemann)

[9] Braess D 2001 *Finite Element* 2nd edn (Cambridge, UK: Cambridge University Press)

[10] Fonov S D *et al* 2004 *New Method for Surface Pressure Measurements Flow-Visualization Conference (University of Notre Dame, Notre Dame, IN, USA)*

Queries

(1) Author: Please be aware that the colour figures in this article will only appear in colour in the Web version. If you require colour in the printed journal and have not previously arranged it, please contact the Production Editor now.
